Supporting information for "Cellulose regeneration and spinnability from ionic liquids"

Lauri K. J. Hauru, Michael Hummel, Kaarlo Nieminen, Anne Michud, Herbert Sixta

Department of Forest Products Technology, Aalto University, School of Chemical Engineering, P.O. Box 16300, 00076 Aalto, Espoo, Finland

+358-50-384 1764

+358-9-470 24259

herbert.sixta@aalto.fi

DBN, 1,5-diazabicyclo[4.3.0]non-5-ene; DWMR, dry-wet modulus ratio; emim, 1-ethyl-3-methylimidazolium; IL, ionic liquid; NMMO, *N*-methylmorpholine oxide; ODE, ordinary differential equation; TMG, tetramethylguanidine

Cross equation fitting

In MatLab, the curve at each temperature was fitted to the Cross model to get the zero-shear viscosity (assuming that the Cox-Merz rule is valid):

$$\eta^* = \frac{\eta_0}{1 + (K\omega)^m} \quad (1)$$

where the input data are η*, the complex viscosity and ω, the angular frequency, and the fitted parameters are η_0, the zero-shear viscosity and the parameters K and m. Shift factors a_T were calculated at each temperature T with:

$$a_T = \frac{\eta_0(T)T_0}{\eta_0(T_0)T} \quad (2)$$

where $\eta_0(T)$ is the zero-shear viscosity at temperature T and $\eta_0(T)$ the same at the reference temperature T_0, which was 70 °C or 95 °C for the NMMO·H_2O reference dope. Reduced angular frequency ω_r and reduced complex viscosity η_r* at reference temperature for each curve are then:

$$\omega_r = a_T \omega \quad (3)$$

$$\eta_r{}^* = \eta^*(\omega, T)\frac{T_0}{a_T T} \quad (4)$$

Shifting all data in this manner gives the master curve, which is then fitted to the Cross model to obtain an improved zero-shear viscosity estimate. (W. P. Cox and E. H. Merz, *Journal of Polymer Chemistry*, 1958, **28**, 619–622; R. J. Sammons, J. R. Collier, T. G. Rials and S. Petrovan, *Journal of Applied Polymer Science*, 2008, **110**, 1175-1181.)

Dope rheology

Although this work is not about dry spin dope, we present also this data for reference. Master curves (Fig. S1) show that all dry ILs have very similar viscosities at high angular frequency. [DBNH]OAc and [emim]OAc (70 °C) are nearly identical, while NMMO·H_2O (95 °C) has a higher zero-shear viscosity (Table S1). Partial regeneration of [emim]OAc with 0.5 or 1.0 n_{H2O}/n_{IL} lowers viscosity at all frequencies, thus crossover points similar to the other solvents occur at lower temperatures (50 °C and 40 °C).

Table S1. Angular frequency (ω), complex viscosity (η*), storage and loss modulus (G'/G") at crossover point, and zero-shear viscosity (η_0) at 70 °C, [a] 95 °C for NMMO

Solvent	T [°C]	Spin?	ω [1/s]	η* [Pa·s]	G'/G" [Pa]	η_0 [Pa·s]
NMMO·H_2O	95	Yes	1.78	3708	4628	18863[a]
[DBNH]OAc	70	Yes	2.31	3268	5316	11109
[TMGH]OAc	80	Yes	0.76	8223	4380	N/A
[emim]OAc	90	Yes	4.06	1708	4884	
[TMGH]OAc	90	No	1.23	4801	4166	N/A
[emim]OAc	70	No	1.34	4882	4625	
[emim]OAc/0.5H_2O	50	No	1.83	3660	4680	5350
[emim]OAc/1.0H_2O	50	No	3.31	2181	5055	3643
[emim]OAc/1.0H_2O	40	>P_{max}	1.75	3984	4900	

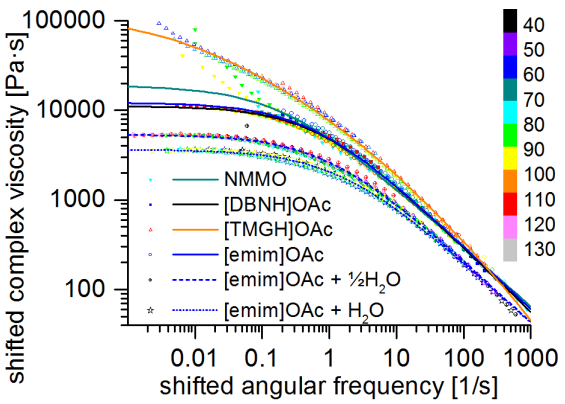

Fig. S1 Master curves of complex viscosity at 70 °C (95 °C for NMMO·H_2O); color scale in °C

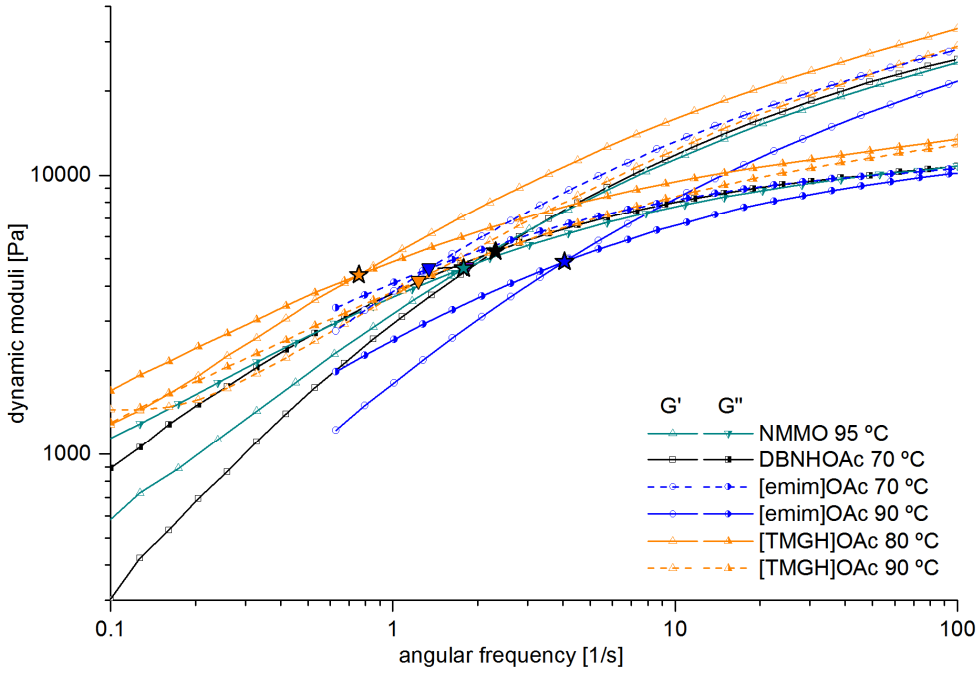

Fig. S2 Dynamic moduli; stars: crossover points, dashed lines and inverted triangles: not spinnable

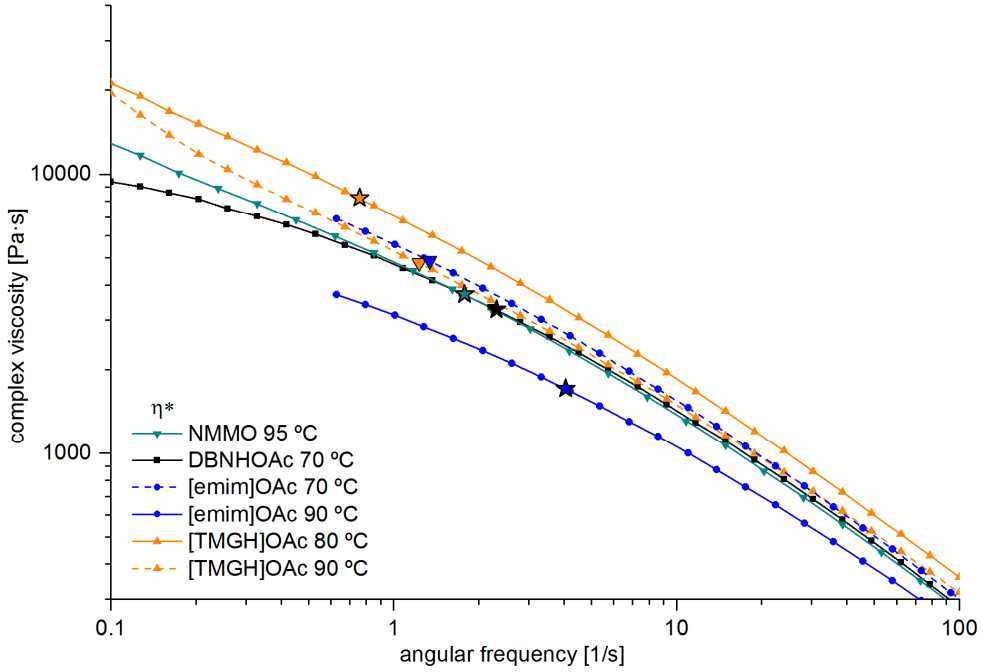

Fig. S3 Complex viscosities; stars: crossover points, dashed lines and inverted triangles: not spinnable

[TMGH]OAc dope has a significantly higher viscosity than other dopes. Within the measured range, the plateau of viscosities at low frequencies characteristic of a Cross fluid could not be detected, and it can be considered as a power law fluid (F.A. Morrison, *Understanding Rheology*, 2001, Oxford University Press, Oxford). <0.1 1/s data for NMMO·H_2O is ignored in the Cross fit. Regardless of these details, the moduli at spinning temperature and at crossover point (Fig. S2) are very similar for all dopes, and crossover points do not diverge too much. Thus, based on the rheological properties of the unhydrated dopes, all solutions should potentially be spinnable.

Table S2. Flow consistency index and power law index for [TMGH]OAc

T [°C]	FCI	m
60	10201	0.67
70	7209	0.62
80	5111	0.57
90	3641	0.53
100	2652	0.49
120	1509	0.41
130	1238	0.42

Rheology and calculation of the master curve for [TMGH]OAc

At the measured range (0.1 to 1000 1/s), the viscosity of [TMGH]OAc dope does not plateau, and therefore it is considered as a power-law fluid (Table S2). However, the [TMGH]OAc dope is not exactly a power-law fluid. A second-degree equation can be used to account for the slight curvature in the log-log plot of viscosity vs. frequency. Because it is not a Cross fluid and has no accessible zero-shear viscosity, a different method must be used to calculate the master curve in Fig. S1. According to the Arrhenius equation, the shift factor a_T at temperature T is the exponential of:

$$\ln a_T = \frac{E_a}{R}\left(\frac{1}{T} - \frac{1}{T_{ref}}\right) \tag{5}$$

where E_a is the activation energy, R = 8.31446 kJ/mol is the universal gas constant and T_{ref} = 343.15 K (70 °C) is the reference temperature. The frequency is shifted by multiplying with a_T, and the viscosity is shifted by $\frac{T_{ref}}{Ta_T}$. With the correct activation energy, the points then fall on a master curve. The shift factors (a_T) were calculated by simultaneously optimizing the Arrhenius activation energy and a fit of a second-degree polynomial to combined data shifted with the given activation energy, using least-squared optimization with Solver in Excel. The resulting master curve has the Arrhenius activation energy of 67663 kJ/mol and is described by the second-degree polynomial:

$$\log \eta = -0.0662 (\log \omega)^2 - 0.542 (\log \omega) + 3.882 \tag{6}$$

As a polynomial interpolation model, the model is not valid at very low (<0.01 1/s) or high (>200 1/s) frequencies.

Modeling the stress-strain curves of gels

The 2nd/3rd degree functions are:

$$\log G'\gamma = \begin{cases} a_1\gamma^2 + b_1\gamma + c_1, & \gamma < \gamma_t \\ a_2\gamma^3 + b_2\gamma^2 + c_2\gamma + d, & \gamma \geq \gamma_t \end{cases} \tag{7}$$

where the free parameters are γ_t, the transition point, and a_n, b_n, …, the polynomial coefficients. By continuity, d is:

$$d = a_1\gamma_t^2 + b_1\gamma_t + c_1 - (a_2\gamma_t^3 + b_2\gamma_t^2 + c_2\gamma_t) \quad (8)$$

Fitting is done in MatLab using the lsqnonlin solver with the initial condition that x_t must be lower than the maximum G'γ. The error function used is the product of logarithmic and linear errors, to give an accurate fit to both the low- and high-strain regions.

Derivation of radial integration

The diffusion simulation produces a map of water content per radius at each time point. The strength and resilience, as measured by rheometry, can be substituted, and thus maps of strength and resilience as a function of radius (S(R), U(R)) are obtained. The total strength of the incipient filament is calculated by numerical integration per radius. The formula is motivated by the following derivation.

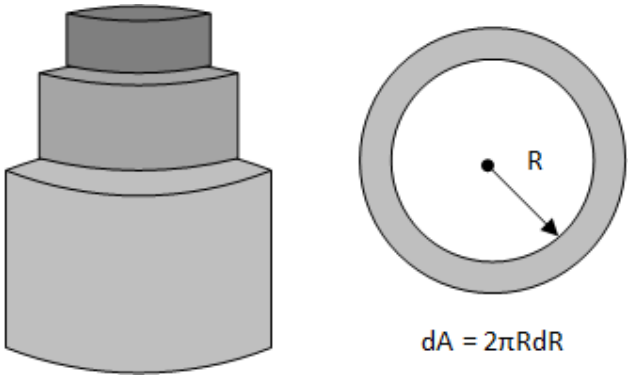

Fig. S4 For integration, the radial layers on a regenerating filament are sectioned into differential annuli, whose strengths are summed up to estimate the strength of the filament

A section of a cylinder is a disc (Fig. S4), and the differential area dA of a thin annulus cut from the disc at radius R is:

$$dA = 2\pi R dR \quad (9)$$

Let us define F as the breaking force and S(R) as the tensile strength as a function of radius. The differential force dF for an annular element of area dA at radius R is:

$$dF = S(R)dA \tag{10}$$

To find the differential force per differential annular element, equation 7 is substituted to equation 8 to obtain equation 9:

$$dF = S(R)\, 2\pi R dR \tag{11}$$

The total breaking force F* is the sum of the differential annular elements and is calculated by integration from 0 to R:

$$F^* = \int dF = \int S(R) 2\pi R dR \tag{12}$$

The tensile strength of the whole filament S* is then

$$S^* = \frac{F^*}{A} = \frac{2\pi \int S(r) R dR}{\pi R_0^2} = \frac{2}{R_0^2} \int S(R) R dR \tag{13}$$

This equation can be simplified by variable substitution. Let us define the dimensionless radius $r = R/R_0$, where R is the real radius at point n and R_0 the filament radius, both in meters. The differential is then $dR = R_0 dr$. Inserting this to the previous equation and noting that $r_0 = 1$ and R_0 is a constant,

$$S^* = \frac{2}{R_0^2} \int_0^{r_0} S(R) r R_0 R_0 dr = 2 \int_0^1 S(R) r dr \tag{14}$$

In practice, in a numerical solution, S(r) and S(R) map one-to-one, because the numerical vector S(r) has the same indices as S(R). Thus, the discrete form of the filament strength is:

$$S^* = 2\sum S(r)rdr \tag{15}$$

where r is a dimensionless radius.

Practical fitting of D_w

Biganska and Navard wrote the equation for water diffusion constant D_w as:

$$\frac{M(t)}{M_\infty} = \frac{4}{\sqrt{\pi}}\sqrt{\frac{D_w t}{l^2}} \tag{16}$$

where M(t) and M_∞ are the masses of water at start and end of diffusion, respectively, l is the sample thickness and t is the time. For small times, $M(t)/M_\infty \approx d(t)/d_\infty$, where d(t) is the distance at time t and d_∞ is the distance travelled when diffusion is complete. This assumption is justified because the water is in plug flow with a sharp front. Thus, the mass diffused out is proportional to the degree of propagation of the front. Thus, we can multiply by sample thickness $l = d_\infty$ to get

$$d(t) = \frac{d(t)}{d_\infty} l = \frac{4}{\sqrt{\pi}}\sqrt{D_w t} \tag{17}$$

The right-hand side is in meters when the units of D_w are m^2/s, and thus left-hand side is multiplied by $l = 10^6$ µm/m to get the distance diffused in µm.

Discretization of the diffusion equations

The discretized form of the spatial part of the diffusion equation is altered slightly depending on whether the diffusivity is constant or variable. The diffusion equation with one spatial coordinate is:

$$\frac{\partial X}{\partial t} = \frac{\partial}{\partial x}\left(D\frac{\partial X}{\partial x}\right) \tag{18}$$

where X is the concentration, x is distance and t is time. The discretized form of the right-hand side of equation 3 is:

$$\frac{D_{i+½}X_{i+1} - (D_{i+½} + D_{i-½})X_i + D_{i-½}X_{i-1}}{(\Delta x)^2} \quad (19)$$

Here the X_i:s denote the concentration values at points separated by the distance Δx on the line. The $D_{i+½}$:s stand for diffusivities at the points halfway between the i:th and i+1:th grid points.

ODE tools in MatLab numerically solve first order ordinary differential equations (ODEs), but the diffusion equation is a partial differential equation with a second order spatial derivative. However, when the spatial domain of the equation is discretized, we can interpret the equation as a system of first order ordinary differential equations. Its solution is the vector of concentrations at each time point at the grid points i.

Discretization for constant diffusivity

If the diffusivity D is constant, equation 18 simplifies to:

$$\frac{\partial \Phi}{\partial t} = D\frac{\partial^2 \Phi}{\partial x^2} \quad (20)$$

For this equation (20) the discretization of the right-hand side is somewhat simpler than equation 19:

$$D\frac{X_{i+1} - 2X_i + X_{i-1}}{(\Delta x)^2} \quad (21)$$

The radial differential and its derivation

For simulating the filament, instead of the linear differential, a radial differential is used:

$$\frac{1}{r_i}D_i\frac{X_{i+1} - X_{i-1}}{2\Delta r} + D_i\frac{X_{i+1} - 2X_i + X_{i-1}}{(\Delta r)^2} \quad (22)$$

where X_i is the concentration and r_i is the dimensionless radius at point i, and Δr is the radial step. The derivation is as follows. The general diffusion equation, where X is the concentration and D is the diffusion constant, is:

$$\frac{\partial X}{\partial t} = \nabla \cdot [D \nabla X] \tag{23}$$

In cylindrical coordinates, the gradient and divergence for some functions f and F are:

$$\nabla f = \frac{\partial f}{\partial r}\hat{r} + \frac{1}{r}\frac{\partial f}{\partial \varphi}\hat{\varphi} + \frac{\partial f}{\partial z}\hat{z} \tag{24}$$

$$\nabla \cdot F = \frac{1}{r}\frac{\partial (rF_r)}{\partial r} + \frac{1}{r}\frac{\partial F_\varphi}{\partial \varphi} + \frac{\partial F_z}{\partial z} \tag{25}$$

where r denotes radial coordinate, φ the azimuthal coordinate and z the axial coordinate. Given cylindrical symmetry, concentrations and thus D are constant in azimuthal direction. Axial diffusion (third term) is slow since axial concentration gradients are small, thus the axial direction can also be ignored. Thus, only the radial coordinate (first term) is used:

$$\frac{\partial X}{\partial t} = \frac{1}{r}\frac{\partial}{\partial r}\left(rD\frac{\partial X}{\partial r}\right) = \frac{1}{r}D\frac{\partial X}{\partial r} + \frac{\partial D}{\partial r}\cdot\frac{\partial X}{\partial r} + D\frac{\partial^2 X}{\partial r^2} \tag{26}$$

If the variation in D is relatively small between individual elements, then the middle term can be ignored. Let us have a 100-point lattice where points are separated by the distance h. Then, the discretization of the differential is:

$$\frac{1}{r_i}D_i\frac{X_{i+1} - X_{i-1}}{2(\Delta x)} + D_i\frac{X_{i+1} - 2X_i + X_{i-1}}{(\Delta x)^2} \tag{27}$$

Diffusion of water

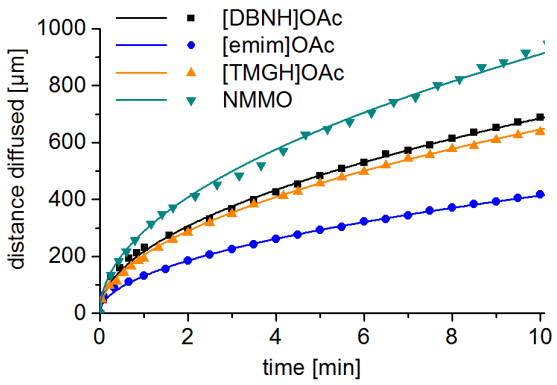

Fig. S5 Diffusion of water into thin layer of dope on a microscope slide

Derivation of the ionic liquid diffusion constant function

A function with the desired properties is:

$$g(X_w) = e^{-aX_w{}^b} \tag{28}$$

where a and b are constants and X_w is the degree of propagation for water (0–1). However, this equation needs to be normalized to the range 0 to 1 by:

$$h(c_w) = \frac{g(X_w) - g(1)}{1 - g(1)} \tag{29}$$

Therefore, for hydrated dopes (positive water content), the equation can be employed to describe the variation from $D_{IL,i}$ to $D_{IL,f}$:

$$D_{IL} = D_{IL,f} + (D_{IL,i} - D_{IL,f})h(X_w), \qquad c_w > 0.001 \tag{30}$$

which reduces to

$$D_{IL} = D_{IL,f} + (D_{IL,i} - D_{IL,f})\frac{e^{-aX_w{}^b} - e^{-a}}{1 - e^{-a}}, \qquad c_w > 0.001 \tag{31}$$

Practical spinnability

13 m-% solutions of dry pulp were prepared. [DBNH]OAc was spinnable up to high D_Rs both in monofilament (100 µm, D_R 7.5 at extrusion velocity of 0.04 ml/min) and multifilament mode. [DBNH]OAc is a known good spinning solvent, since we have spun [DBNH]OAc dopes up to D_R 17, giving filaments with very high tenacity (870 MPa) and high modulus (32 GPa) (Hauru LKJ, Hummel M, Michud A, Sixta H (2014) Dry jet-wet spinning of strong cellulose filaments from ionic liquid solution. Cellulose 20 (6):4471-4481. doi:10.1007/s10570-014-0414-0). [TMGH]OAc was not spinnable at 0.04 ml/min, and barely spinnable at 0.02 ml/min at D_R 2, with filament breaks occurring when attempting higher D_Rs. It was spinnable only at 80 °C, but not at 70, 90 or 100 °C, even if its crossover point at 90 °C is similar to [DBNH]OAc. Since it was often possible to spin for a short while, it appears that break was caused by draw resonance. With lower dope concentration (10%), the incipient filament was very weak and simply crumbled when touched. [Emim]OAc (15 m-%) was not spinnable with the 100 µm spinneret at all in this system (0.01–0.05 ml/min), regardless of D_R or temperature (50–70 °C). A telescope-type breach occurred: a skin of regenerated gel formed, but it ruptured exposing the fluid interior leading to progressive thinning and failure. We tried adding 0.5 and 1.0 equivalents per IL of water to the spin dope (30–60 °C and 40–50 °C, with similar rheology), to no avail. Telescope-type breach occurred at 40 °C and at 50 °C with v_e 0.02 ml/min. With v_e 0.04 ml/min, cohesive breaks occurred in the bath for 0.5 n_{H2O}/n_{IL} at 50–60 °C and for 1.0 n_{H2O}/n_{IL} at 40–50 °C. For [emim]OAc, with a 250 µm spinneret at 90 °C, a stable filament could be maintained up to D_R 3. This D_R is too low to be technically useful and the filaments appeared amorphous and weak. NMMO·H_2O, a known good spinning solvent, was spun in multifilament mode with a 100 µm spinneret at a temperature of 95 °C, in our experiment up to D_R of 6. [McCorsley, C.C. III (1981) Process for shaped cellulose article prepared from a solution containing cellulose dissolved in a tertiary amine N-oxide solvent, United States Patent 4246221 A, 1981-01-20.]

See last page for the filament properties.

Gel strengths and yield strains

Water percentage and stoichiometry are related by Eq. 1:

$$\frac{n_{H2O}}{n_{IL}} = \frac{w_w/M_w}{(100\% - w_{cellu} - w_w)/M_{IL}} \quad (32)$$

where w_w is water percentage, w_{cellu} cellulose content, and M_w and M_{IL} are the molar masses of water and the IL.

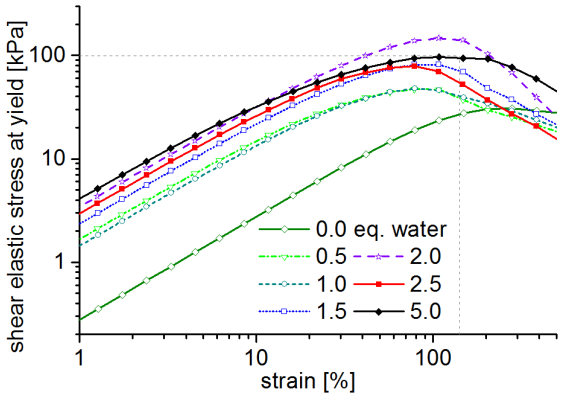

Fig. S6 Shear stress-strain curves of [DBNH]OAc dopes mixed with water and the yield stress and yield strain (gray dashed lines) identified for the curve with 5.0 eq water

Solidification of the gel is immediate with 0.5 equivalents of water added (0.5 n_{H2O}/n_{IL}), as evidenced by the rapid drop in yield strain shown in Fig. S6: the material becomes inelastic and more brittle. The yield strain is high (170–450%) for the dry dope, but low (80–200%) and remains approximately constant with increasing water content. The exception is [emim]OAc, for which it rises from 0.5 to 2.5 n_{H2O}/n_{IL}.

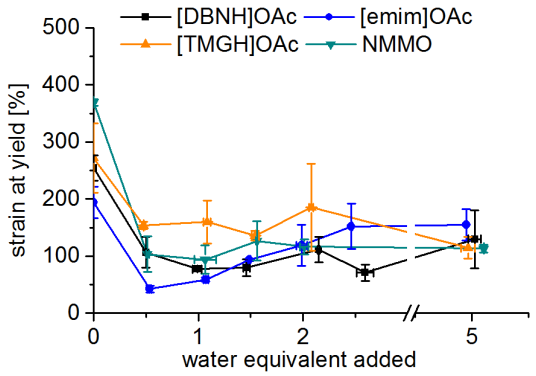

Fig. S7 Strain at yield vs. water added.

Gel strength, defined as elastic stress at yield, varies both with IL and water content. The gel strengthens within 0.5 n_{H2O}/n_{IL} in NMMO·H_2O (0–0.5 n_{H2O}/n_{IL}) and in [TMGH]OAc (0.5 and 1 n_{H2O}/n_{IL}). In [DBNH]OAc, gel strength remains the same until 1.0 n_{H2O}/n_{IL}, peaks at 2.0 n_{H2O}/n_{IL} and attains its final value at 2.5 n_{H2O}/n_{IL}. Only [emim]OAc has a "valley" of lower strength at 0.5 n_{H2O}/n_{IL}, preceded by stronger dry dope, and followed by gel strength development from 0.5 to 2.0 n_{H2O}/n_{IL} (Fig. S7).

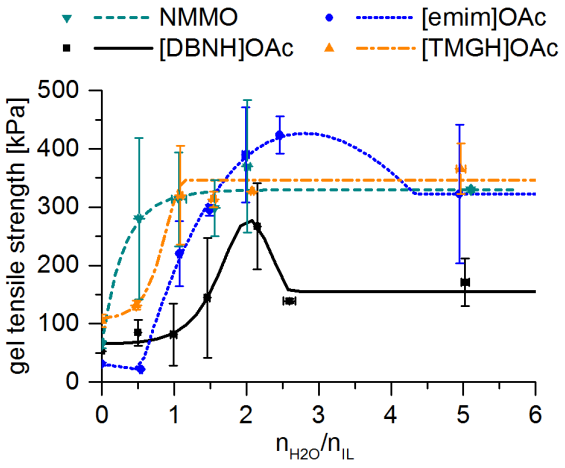

Fig. S8 Gel tensile strength vs. water added and the interpolation functions used in simulations

Elastic resiliences have a similar trend as the gel strengths (Fig. 1): [emim]OAc has extremely low resilience at 0.5 n_{H2O}/n_{IL}, but the final gel of [DBNH]OAc is the least resilient. [Emim]OAc does have the lowest resiliences of all at 0–1 n_{H2O}/n_{IL}.

For the simulations, piecewise interpolation functions based on the raw strength and resilience data are used for strength and resilience (Figs 1 and S7). For strength, the initial part is modeled with a hyperbolic secant function for [TMGH]OAc and [DBNH]OAc, a parabola for [emim]OAc and an vertically inverted exponential decay for NMMO·H_2O. The final part is a constant function. Resilience data are modeled using a piecewise function consisting of a parabola and a constant function.

Elastic moduli

The elastic moduli are shown in Fig. S8. The ultimate moduli are similar and develop below 1 n_{H2O}/n_{IL}, except for [DBNH]OAc, for which it is consistently lower at all water contents and requires the highest water content (2.1 n_{H2O}/n_{IL}) to develop.

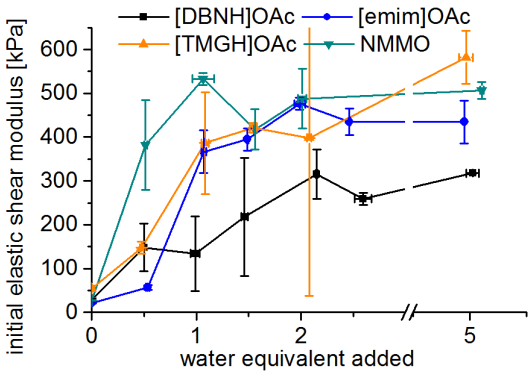

Fig. S9 Initial modulus in shear vs. water added.

Motivation of the filament speed and diameter used

The simulation was run with incipient filament diameters and speeds that would be realistic in spinning. Incipient filament diameter is:

$$d = 2\sqrt{\frac{r_0^2}{D_R}} \tag{33}$$

This is not the final diameter, since washing the IL out and drying causes the fiber to shrink. The extrusion velocity (v_e, in m/min) is calculated from the extrusion flow rate (V_e, in ml/min):

$$v_e = \frac{V_e}{A_0} = \frac{V_e}{\pi r_0^2} \tag{34}$$

Then, the incipient filament velocity (v_1) is simply:

$$v_1 = v_e D_R \tag{35}$$

Realistic extrusion velocities per nozzle are around 0.05 ml/min, and Lyocell spinning is typically run at D_Rs of 10–20. For D_R 10 and V_e 0.05 ml/min with a d_0 = 100 µm spinneret, the wet filament diameter decreases from 100 to 31.6 µm in the air gap, and godet velocity is v_1 = 63.7 m/min. Therefore, the filament radius 15.3 µm is chosen for the simulations.

Dependencies of regeneration depth on draw ratio and velocity

The Crank solution to the diffusion equation for water (Eq. 3) is solved for time where the diffusion front has reached the filament radius, or d = l = r, to yield the regeneration time. Drawn jet radius (r_1) is calculated from $r_1^2 = r_0^2/D_R$ and substituted. It is assumed all drawing occurs in the air gap, as the regenerated filament is stronger than the jet and transfers the stress to the jet. [S. A. Mortimer and A. A. Péguy, *Cellul. Chem. Technol.*, 1996, **30**, 117-132.]

$$t_{reg} = \frac{\pi r_0^2}{16 D_w D_R} \tag{36}$$

Drawn jet velocity (v_1) is by definition $v_1 = D_R v_e$. The regeneration depth (Δx_{reg}), or the length travelled by the jet while regenerating is simply $\Delta x_{reg} = v_1 t_{reg}$. Substituting t_{reg} then v_1, D_R cancels out:

$$\Delta x_{reg} = \frac{v_1 \pi r_0^2}{16 D_w D_R} = \frac{v_e D_R \pi r_0^2}{16 D_w D_R} = \frac{v_e \pi r_0^2}{16 D_w} \tag{37}$$

Thus, regeneration depth is not a function of D_R, but is a linear function of v_e. This is seen in the simulation, confirming its validity.

Diffusion diagrams

An example of a strength profiles at various depths is illustrated in Fig. S9. The total strength is the radial integral of each curve. The full set of curves is depicted as a heatmap in Fig. S10, wherein curves in Fig. S9 represent slices of the map at the depths shown.

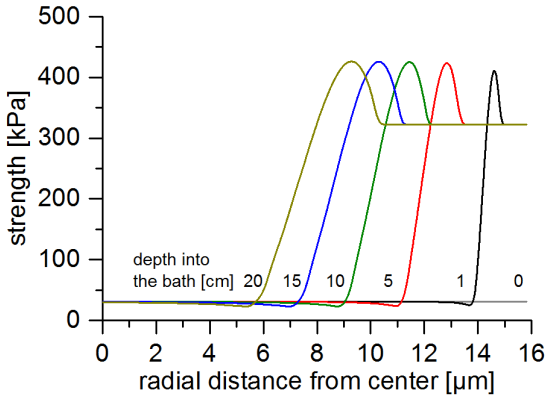

Fig S10. Strength profiles of slices of a [emim]OAc filament at various depths in the bath; the radially weighted integrals of the curves give the overall strengths of the incipient filament

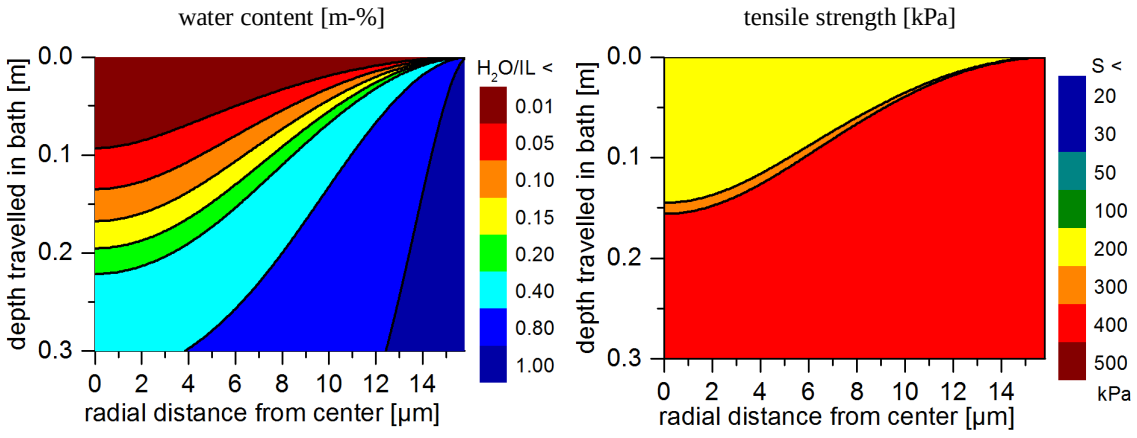

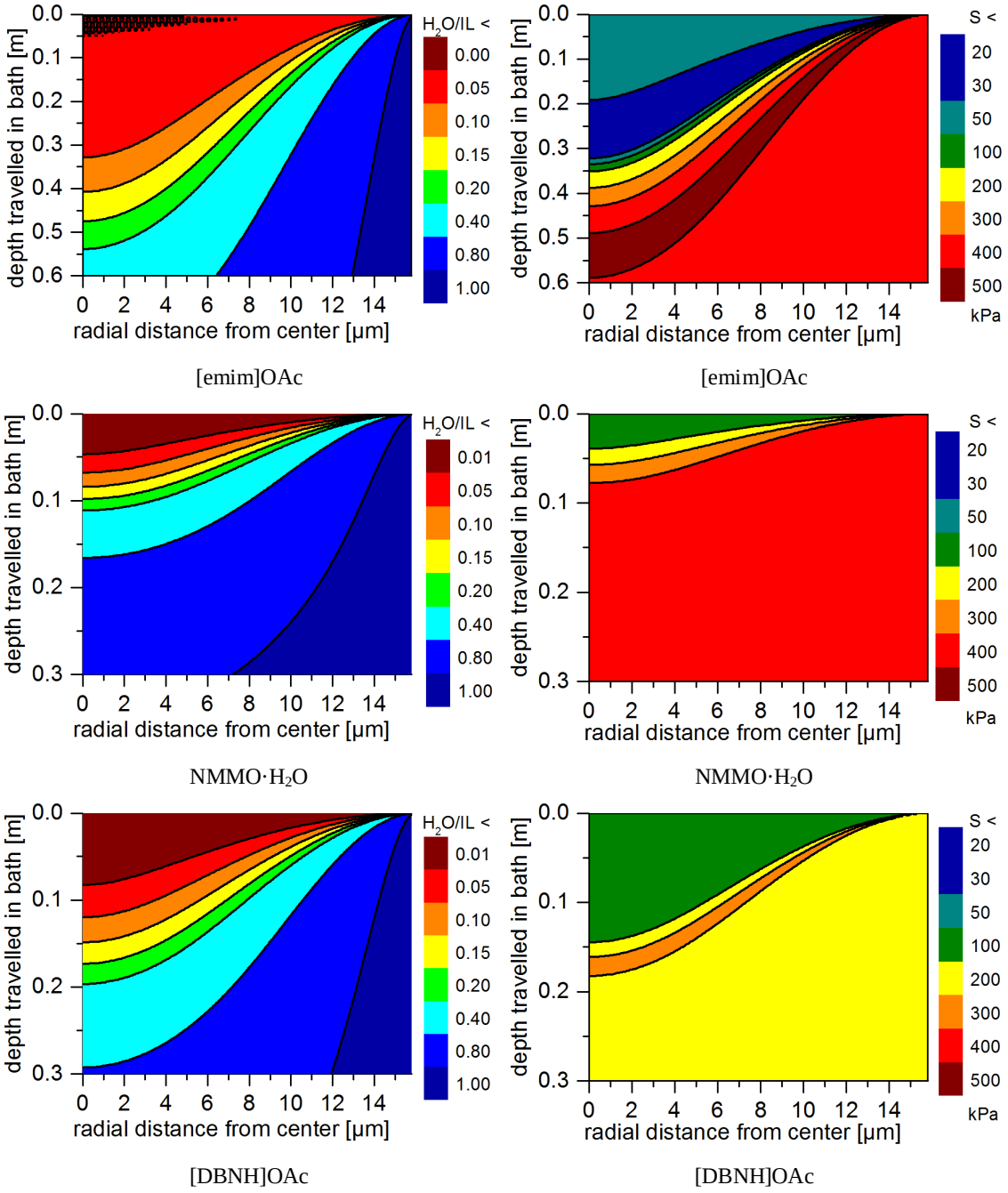

Fig. S11 Simulated radial distributions of water to dope ratio and minimum gel strength in a filament moving through the bath at 63.7 m/s (V_e = 0.05 ml/min at D_R = 10) for each dope; note [emim]OAc with longer depth scale

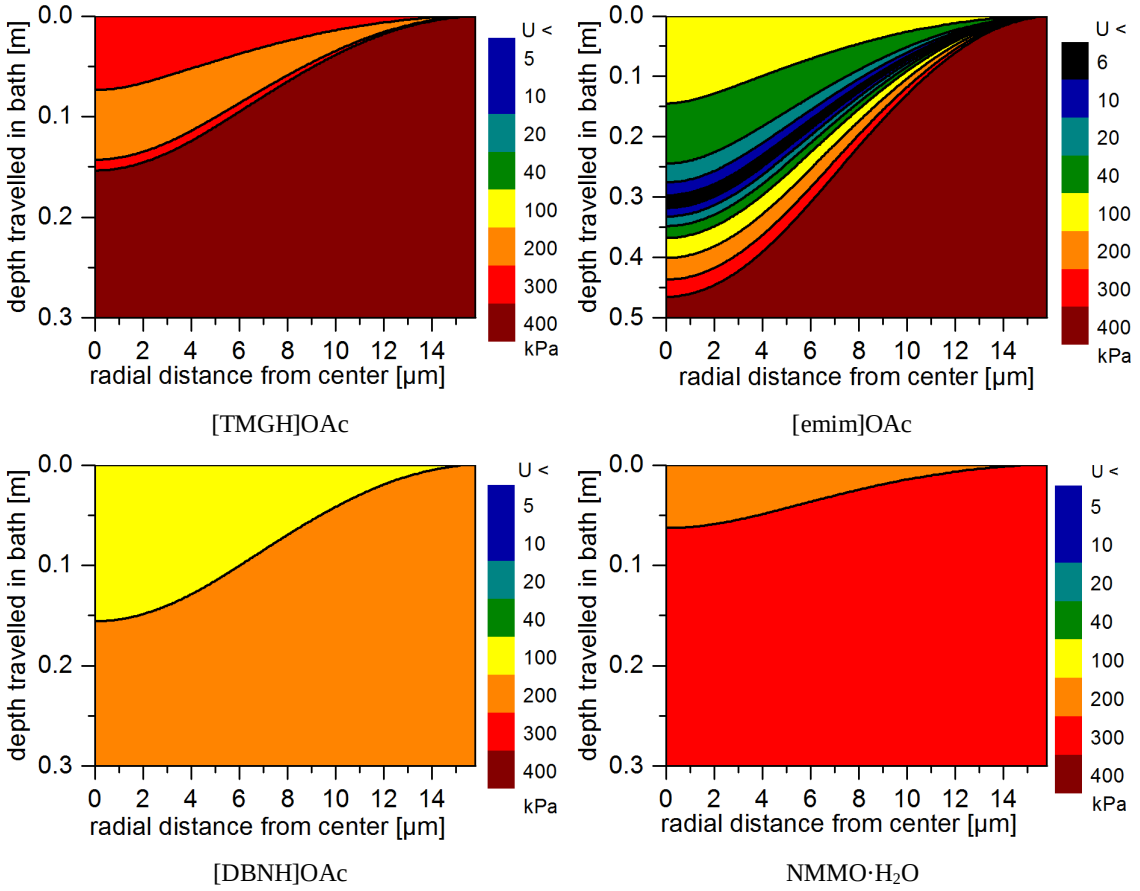

Fig. S12 Simulated radial distributions of minimum resilience in a filament moving through the bath at 63.7 m/s (V_e = 0.05 ml/min at D_R = 10) for each dope; note [emim]OAc with longer depth scale

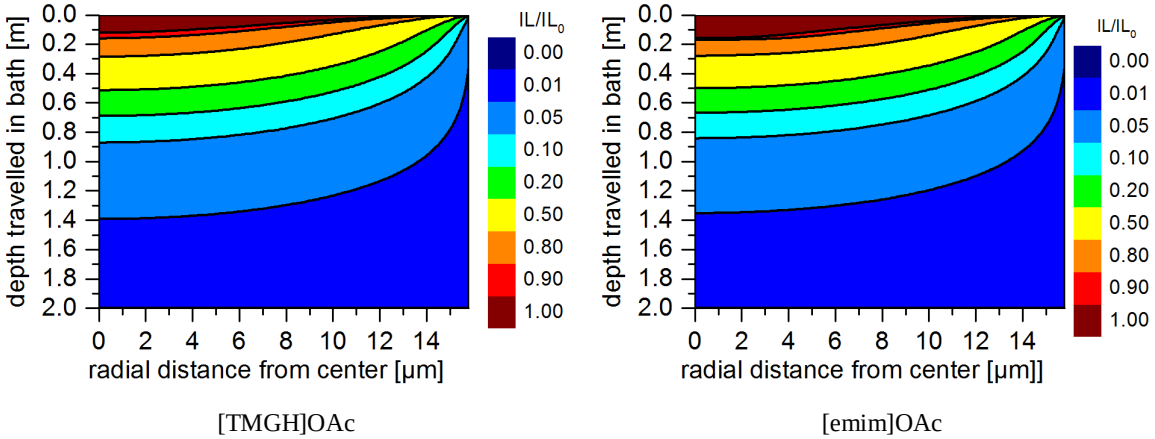

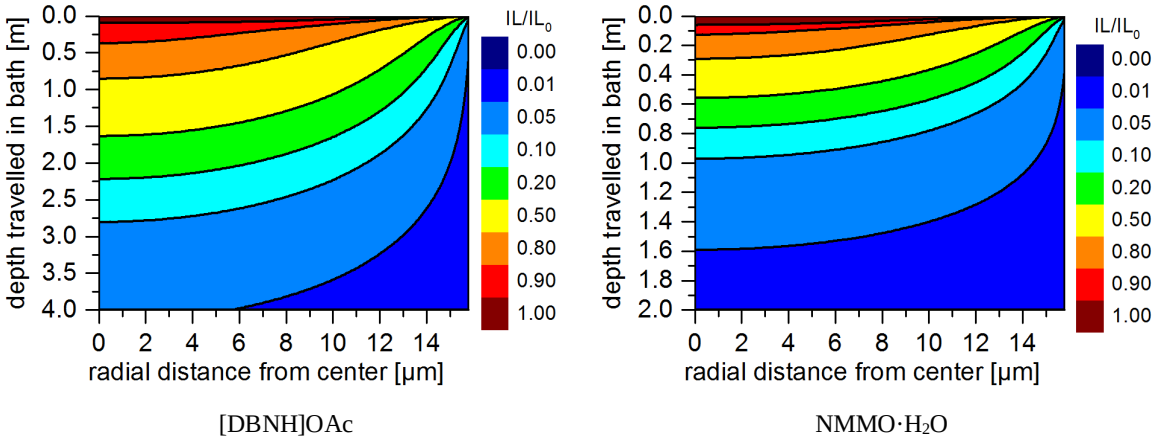

Fig. S13 Simulated radial distributions of remaining ionic liquid in a filament moving through the bath at 63.7 m/s (V_e = 0.05 ml/min at D_R = 10) for each dope; notice [emim]OAc with longer depth scale

Washing simulation

Although the initial changes in D_{IL} are fast, removing the ionic liquid in one bath would require considerable residence times. Given the conditions D_R 10, V_e 0.05 ml/min, d_0 = 100 µm spinneret, wet filament diameter d = 31.6 µm, v_1 = 63.7 m/min and bath temperature 15 °C, removing 99% of the ionic liquid in a single bath would require a bath length of 3.5 m for [DBNH]OAc, 1.2 m for NMMO·H_2O and 1.0 m for others (Fig. S13). However, in an industrial spinning process, there first a regeneration bath followed by multiple washing baths, with separately controlled temperatures and solvent contents. Therefore, modeling the washing with one bath at a single temperature is not technically relevant.

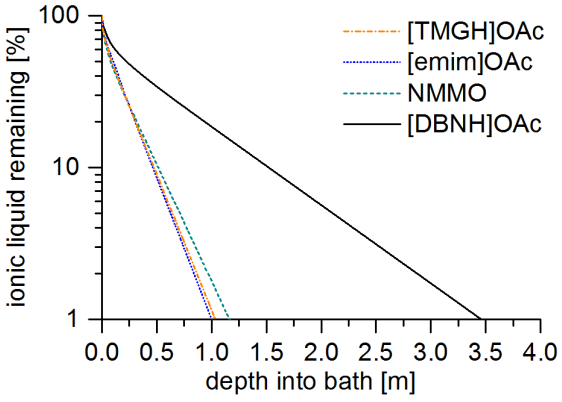

Fig. S14 Simulated diffusion of ionic liquid from a filament into the bath

Filament properties

Table S3. Filament properties obtained from fiber spinning

solvent	D_R	titer [dtex]	tenacity [cN/tex]	ten. wet [cN/tex]	elongation [%]	elong. wet [%]	elastic limit [%]	modulus [cN/tex]	mod. wet [cN/tex]	orientation [%]	prop limit [%]	resilience [MJ/m³]
[emim]OAc	1.1	99.6±5.8 (5.9%)	11.7±0.5 (4.2%)	5.8±0.7	65.3±4.8	57.0±9.7	1.3±0.1	501±61	15±2	32±2	1.30±0.13	0.64±0.20
250 µm	1.5	66.8±4.6 (6.8%)	13.2±0.7 (5.2%)	6.6±0.7	44.6±5.3	33.5±3.1	1.2±0.0	529±20	31±4		1.20±0.05	0.57±0.07
0.5 ml/min	2.0	65.1±4.2 (6.4%)	11.6±0.7 (5.7%)	6.2±0.8	41.0±3.8	30.6±4.4	1.1±0.2	373±57	31±3		1.06±0.16	0.31±0.14
90 °C	2.2	66.3±5.0 (7.5%)	12.1±0.8 (6.7%)	6.0±1.3	40.7±4.4	30.1±6.9	1.3±0.1	470±39	32±5	40±9	1.30±0.05	0.60±0.10
	2.3	64.1±4.9 (7.7%)	10.3±0.9 (9.1%)	6.0±0.6	35.8±2.0	26.3±3.9	1.1±0.1	473±42	37±5		1.11±0.09	0.43±0.11
	2.5	56.1±4.4 (7.8%)	12.6±0.5 (4.0%)	6.8±0.8	35.3±3.3	33.5±3.3	1.5±0.2	443±46	27±5		1.47±0.20	0.72±0.27
	2.7	49.1±5.1 (10.3%)	12.6±1.0 (8.0%)	6.8±0.6	26.6±4.9	30.4±2.6	1.7±0.1	318±40	30±5		1.75±0.11	0.73±0.19
	2.9	44.4±1.7 (3.9%)	13.9±1.6 (11.8%)	6.6±1.2	25.3±5.7	26.5±4.1	1.8±0.2	329±50	33±4	44±1	1.83±0.22	0.83±0.33
[DBNH]OAc	1.0	24.0±3.0 (12.6%)	18.9±2.0 (10.7%)	12.9±2.2	16.3±2.8	21.7±4.4	1.3±0.1	695±98	86±15	57±2	1.32±0.12	0.91±0.29
100 µm	3.0	7.9±1.2 (14.5%)	35.1±4.4 (12.4%)	25.4±1.9	9.7±1.2	13.8±1.8	1.0±0.0	1311±170	230±25	70±3	1.02±0.04	1.03±0.22
0.04 ml/min	5.0	5.4±1.4 (26.3%)	38.8±5.9 (15.1%)	27.7±5.4	8.6±1.6	11.7±2.1	1.0±0.0	1502±204	282±44	72±11	1.00±0.05	1.12±0.26
70 °C	7.5	3.0±0.9 (30.0%)	38.5±8.4 (21.9%)	27.2±6.1	7.9±1.7	8.9±1.9	1.0±0.0	1445±105	320±110	68±4	1.04±0.04	1.18±0.17
[TMGH]OAc	2.0	15.5±0.9 (5.9%)	10.9±1.1 (10.2%)	3.3±0.3	9.3±1.0	11.1±1.1	1.3±0.2	460±98	40±4	unoriented	1.26±0.20	0.54±0.29
100 µm 0.02 ml/min 80 °C												
NMMO	1.4	14.1±1.5 (10.8%)	22.7±2.8 (12.4%)	14.8±1.0	16.8±5.8	19.3±3.4	1.1±0.1	833±163	97±18	56±5	1.14±0.08	0.81±0.28
100 µm	2.0	11.1±2.3 (20.4%)	24.6±3.4 (13.6%)	19.5±1.6	11.5±1.6	12.7±1.7	1.1±0.2	924±125	187±26	65±4	1.07±0.15	0.79±0.34
0.01 ml/min	2.8	6.6±0.9 (13.3%)	27.0±4.3 (16.1%)	20.4±2.3	9.9±2.3	13.3±2.2	1.0±0.1	1065±102	179±19		0.99±0.07	0.79±0.19
95 °C	4.8	5.0±0.4 (8.0%)	31.6±2.2 (6.8%)	24.7±4.1	8.8±1.2	12.3±2.9	1.0±0.1	1229±95	245±42		0.97±0.10	0.87±0.25
	4.7	4.4±0.6 (12.5%)	30.3±7.5 (24.6%)	24.7±2.9	8.9±2.8	13.1±2.7	0.9±0.0	1135±80	210±30		0.92±0.05	0.72±0.12
	5.1	3.7±0.4 (9.6%)	31.7±5.5 (17.2%)	24.8±5.1	9.3±1.4	12.4±2.5	0.9±0.1	1172±144	232±37	61±8	0.95±0.09	0.79±0.25
	5.6	3.1±0.5 (17.3%)	32.6±4.6 (14.0%)	28.0±2.7	8.2±2.4	13.0±1.9	0.9±0.1	1373±131	262±52		0.94±0.14	0.91±0.36
	6.2	3.7±0.7 (18.8%)	31.2±6.6 (21.1%)	26.8±2.8	8.7±2.4	11.3±2.0	0.8±0.2	1365±226	258±57	68±4	0.83±0.20	0.71±0.46